Appendix A. Supplementary Material

Mineralization kinetics of biosiliceous sediments in hot subseafloors

Ivano W. Aiello [a] , Tobias W. Höfig [b], Armelle Riboulleau [c], Andreas P. Teske [d], Daniel Lizarralde [e], Jeanine L. Ash [f], Diana P. Bojanova [g], Martine D. Buatier [h], Virginia P. Edgcomb [e], Christophe Y. Galerne [k], Swanne Gontharet [j], Verena B. Heuer [k], Shijun Jiang [l], Myriam A.C. Kars [b,m], Ji-Hoon Kim [n], Louise M.T. Koornneef [o], Kathleen M. Marsaglia [p], Nicolette R. Meyer [q], Yuki Morono [r], Raquel Negrete-Aranda [s], Florian Neumann [ad], Lucie C. Pastor [t], Manet E. Peña-Salinas [u], Ligia L. Pérez-Cruz [v], Lihua Ran [w], John A. Sarao [x], Florian Schubert [y], S. Khogenkumar Singh [z], Joann M. Stock [aa], Laurent Toffin [t], Wei Xie [l], Toshiro Yamanaka [ab], Guangchao Zhuang [ac]

a *San Jose State University, Moss Landing Marine Laboratories, Moss Landing, CA 95039, USA*

b *International Ocean Discovery Program, Texas A&M University, College Station, TX 77845, USA*

c *Laboratoired'OcéanologieetdeGéosciences,UMR8187,UniversitédeLille,CNRS,Villeneuved'Ascq59655,France*

d *Department of Earth, Marine and Environmental Sciences, University of North Carolina at Chapel Hill, Chapel Hill, NC 27599, USA*

e *Department of Geology and Geophysics, Woods Hole Oceanographic Institution, Woods Hole, MA 02543, USA*

f *Department of Earth, Environmental and Planetary Sciences, Rice University, Houston, TX 77005, USA*

g *Department of Earth Sciences, University of Southern California, Los Angeles, CA 90089, USA*

h *Chrono-Environnement, UMR 6249-CNRS, Université Bourgogne Franche-Comté, Besançon 25030, France*

i *Faculty of Geosciences, University of Bremen, 28359 Bremen, Germany*

j *LOCEAN UMR 7159 Sorbonne Université/CNRS/IRD/MNHN, 4 place Jussieu – boîte 100, F-75252 Paris, France*

k *MARUM – Center for Marine Environmental Sciences, University of Bremen, Bremen, Germany*

l *College of Oceanography, Hohai University, Nanjing, China*

m *Center for Advanced Marine Core Research, Kochi University, Nankoku-shi 783-8502, Japan*

n *Marine Geology & Energy Division, Korea Institute of Geoscience & Mineral Resources (KIGAM), Daejeon 305-350, Republic of Korea*

o *Earth and Environmental Sciences, School of Geography, University of Plymouth, Plymouth, Devon PL4 8AA, United Kingdom*

p *Department of Geological Sciences, California State University, Northridge, CA 91330-8266, USA*

q *Department of Earth System Science, Stanford University, Stanford, CA 94305, USA*

r *Kochi Institute for Core Sample Research, Institute for Extra-cutting-edge Science and Technology Avant-garde Research (X-star), Japan Agency for Marine-Earth Science and Technology, Nankoku Kochi 783-8502, Japan*

s *Investigador por Mexico, Department of Geology, CICESE, Ensenada, BC 22860, Mexico*

t *IFREMER, Centre de Brest, 29280 Plouzané, France*

u *Department of Coastal Oceanography, UABC, Zona Playitas, Ensenada, BC 22860, Mexico*

v *Institute of Geophysics, Universidad Nacional Autónoma de México (UNAM), Mexico City 04510, Mexico*

w *The Second Institute of Oceanography, Ministry of Natural Resources, Laboratory of Marine Ecosystem and Biogeochemistry, Hangzhou, China*

x *College of Geosciences, Texas A&M University, College Station, TX 77843, USA*

y *Section Geomicrobiology, GFZ German Research Centre for Geosciences, Telegrafenberg, 14473 Potsdam, Germany*

z *National Centre for Antarctic and Ocean Research (NCAOR), Department of Geoscience, Vasco-da-Gama, Goa 403804, India*

[aa] *Division of Geological and Planetary Sciences, California Institute of Technology, Pasadena, CA 91125, USA*

[ab] *Department of Ocean and Environmental Sciences, Tokyo University of Marine Science and Technology, Tokyo, 108-8477, Japan*

[ac] *Laboratory for Marine Ecology and Environmental Science, Qingdao National Laboratory for Marine Science and Technology, Qingdao, 266237, China*

[ad] *GFZ, German Research Centre for Geosciences, Section 4.8 Geoenergy, Telegrafenberg, 14473 Potsdam, Germany*

Figure S1

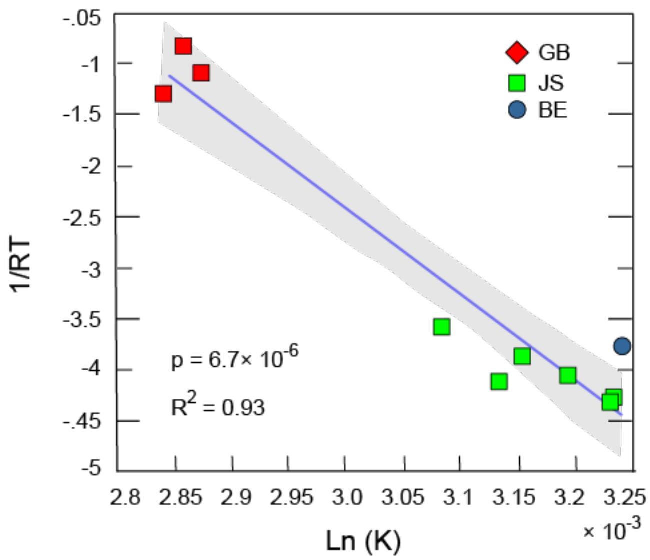

Figure S1. Best fit for ln(k) as a function of 1/RT to calculate the kinetic parameters A and Ea for the Guaymas Basin sites (red), the Sea of Japan Sites (green) and the Bering Sea site (blue); see Tab. 4 in the main text. The gray bands show the 95% confidence intervals.

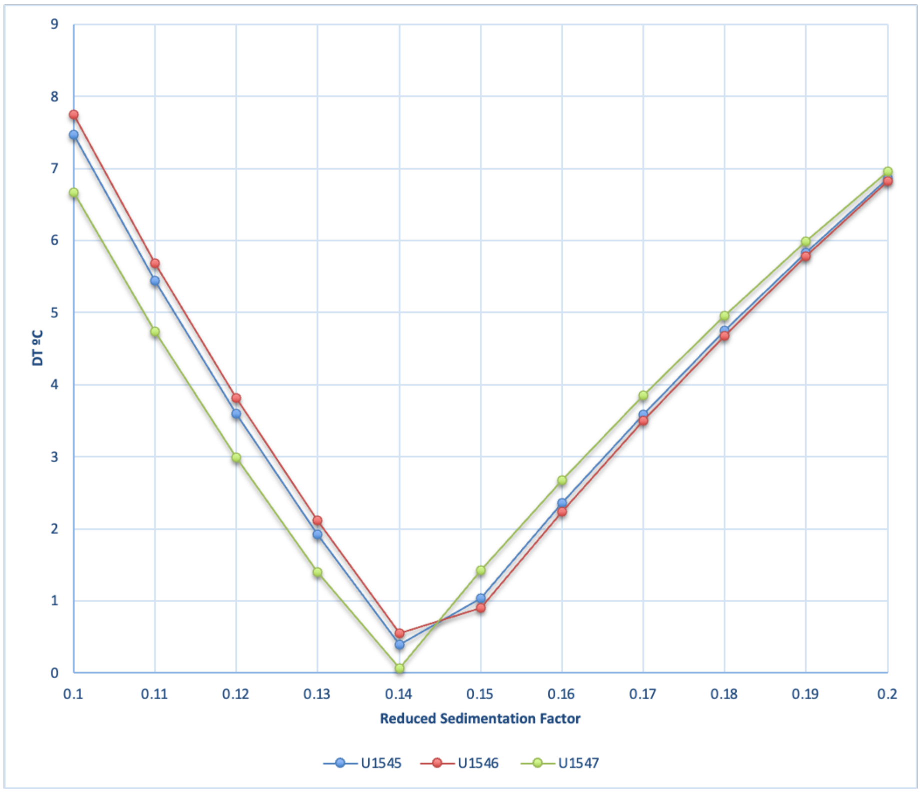

Figure S2. The figures shows the results of a subset of runs of the simulations to test the hypothesis that the rapid sedimentation rates are responsible for shuttling amorphous silica deeper/older than expected based on current kinetic models. For this purpose, the temperatures for opal-CT precipitation were calculated by simulating about one order of magnitude slower sedimentation rates. The latter was simulated by reducing the time factor (t) in $k = -\ln(0.9)/t$ to a value between 0.1 and 0.2. The best fit between observed and modeled data (expressed as the difference in temperature between the two; DTºC in the Y-axis) occurs when ~14% slower sedimentation rates are used ('reduced sedimentation rate' in x-axis; see also Tab. S4).

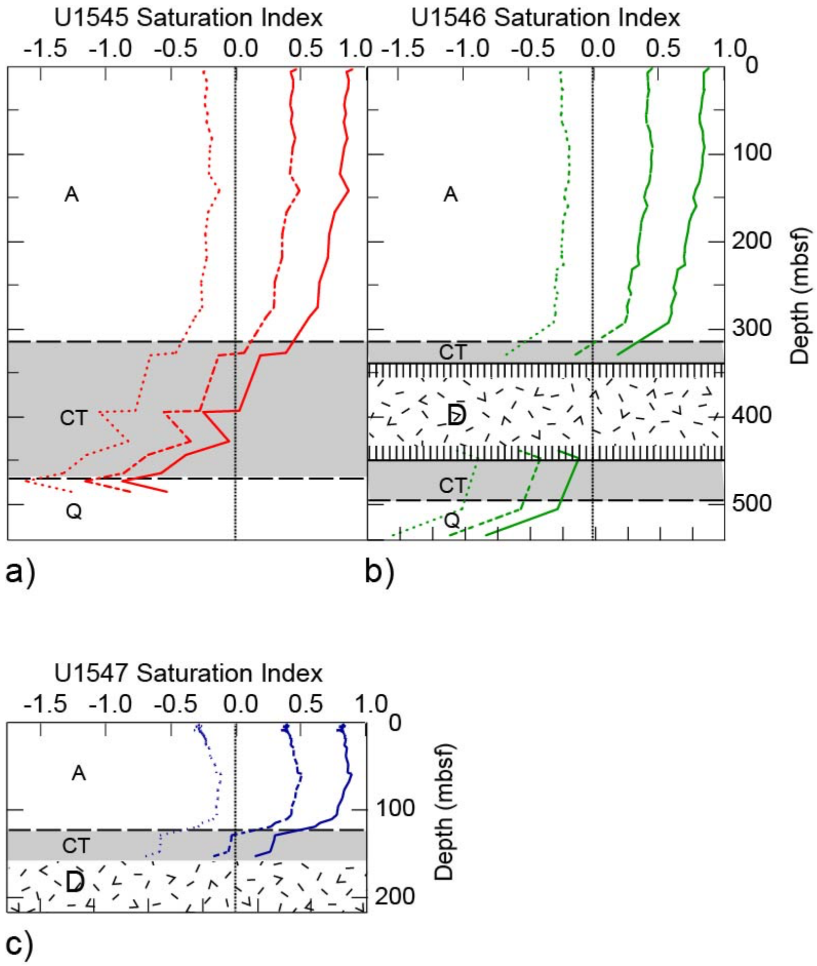

Figure S3. Saturation indexes with respect to the three main silica phases for Sites U1545 (red), U1546 (green) and U1547 (blue). The dotted lines represent the SI for opal-A, the dashed lines for opal-CT, and the solid lines for quartz. SI is the log of the ration between the Ion Activity Product (i.e. porewater silica concentration) and the solubility constant of the three main silica phases calculated using Gunnarsson and Arnorsson (2000) solubility equations. SI=0 indicates saturation, S>0 supersaturation and S<0 undersaturation. The minimum in the silica concentration profile near the seafloor is due to the fact that silica is strongly undersaturated in seawater. Lithological symbols: the letters represent the main silica phases (A = opal-A, CT = opal-CT, Q = quartz), and intrusive dolerite bodies (D). The vertical dashed lines show the approximate extent of the metamorphic contact aureole associated with the massive mafic sill at Site U1546.

Table S1 - Silica Porewater data

Site U1545^ (mbsf)	Si (µM)	Site U1546 (mbsf)*	Si (µM)	Site U1547 (mbsf)**	Si (µM)
2.97	791.79	1.76	748.74	0.5	664.93
5.95	729.86	6.93	711.24	1	650.68
15.45	809.7	15.69	753.5	2	653.2
24.96	853.53	25.78	805.13	2.5	700.21
34.45	869.03	25.78	816.95	2.96	630.58
43.95	907.12	34.81	834.4	3.51	650.86
53.45	993.54	45.6	880.6	4.01	679.76
62.96	1019.91	53.7	908.77	4.81	698.88
72.36	1116.32	53.7	899.79	5.8	681.01
81.86	1224.61	63.94	963.85	6.3	700.48
91.59	1236.43	74.31	1085.52	7.3	644.23
122.39	1386.3	82.79	1145.82	7.8	736.19
141.46	1811.18	91.8	1244.61	8.26	707.22
165.92	1640.38	103.01	1288.74	8.81	731.31
191.28	1723.33	112.31	1358.84	9.31	744.32
218.25	1956.05	120.94	1397.99	10.31	765.33
245.85	1960.64	131.61	1448.64	10.81	771.09
274.71	2208.22	140.11	1428.35	11.81	782.11
285.82	2021.77	149.64	1447.5	12.31	802.8
326.73	1641.47	159.24	1609.72	13.31	816.76
329.62	1059.03	168.52	1573.49	13.81	825.04
392.85	984.74	177.54	1578.45	14.66	840.32
394.25	523.92	187.51	1635.43	15.55	836.41
427.73	958.95	197.73	1676.37	17.05	874.46
443.26	478.95	205.4	1708.73	17.76	896.03
463.97	338.34	212.12	1764.43	18.56	892.11
473.16	176.88	216.78	1787.06	20.06	916.65
485.34	408.67	226.17	1915.43	21.56	928.73
		231.54	1733.07	23.06	939.2
		238.48	1766.38	24.56	960.98
		243.14	1784.71	27.26	1043.4
		252.56	1798.47	36.76	1174.77
		258.82	1932.86	46.25	1404.29
		273.41	1922.36	55.76	1583.59
		281.46	2017.27	57.03	1733.22
		292.18	2011.93	66.11	1865.08
		328.85	981.53	75.45	1943.55
		438.35	566.02	84.81	2123.92
		447.03	842.23	94.25	2222.69
		505.09	735.33	103.85	2444.96
		535.1	232.93	108.89	2371.18
				113.1	2025.25
				117.34	1959.89
				127.3	1078.6
				131.48	1126.59
				145.93	1230.05
				151.14	995.11

Notes: ^The dataset for Site U1545 is from Hole A; *The dataset for Site U1546 combines porewater data from Holes B and C; **The datset for Site U1547 combines porewater data from Holes A and B

Table S1. Concentration of porewater silica (in μM) obtained from IODP X385 Sites U1545, U1546, and U1547.

Table S2 - *In situ t*emperature data

Site U1545^ (mbsf)	T°C	Tool	Site U1546* (mbsf)	T°C	Tool	Site U1547** (mbsf)	T°C	Tool
0	3.85		0	3.96				
33.3	10.88	APCT-3	32.3	10.05	APCT-3	24.3	25.65	APCT-3
60.8	17.32	APCT-3	60.8	16.3	APCT-3	34.7	27.97	APCT-3
89.3	24.56	APCT-3	89.3	22.4	APCT-3	52.8	37.36	APCT-3
117.8	31.04	APCT-3	117.8	28.14	APCT-3	71.8	49.68	APCT-3
138.1	36.17	APCT-3	146.3	35.19	APCT-3	90.8	56.25	APCT-3
161.4	46.89	APCT-3	174.8	41.66	APCT-3	101.9	66.83	SET2
189.4	47.63	APCT-3	198.5	45.98	APCT-3	124.2	74.21	SET2
189.4	47.92	APCT-3	218.4	51.12	APCT-3			
217.6	54.37	APCT-3	239.9	54.44	SET2			
218.6	54.95	APCT-3	259.4	61.08	SET2			
246.8	62.47	APCT-3	288.7	66.93	SET2			
275	67.54	APCT-3						
287.9	67.47	SET2						
288.9	71.17	SET2						
329.5	77.58	SET2						
358.6	85.22	SET2						

Notes: ^The dataset for Site U1545 is from Hole B; *The dataset for Site U1546 is from Hole A; **The dataset for Site U1547 is from Hole B

Table S2. *In situ* temperature data for the IODP X385 drill sites presented in this study. APCT-3 = Advanced Piston Corer Temperature 3 tool; SET2 = Sediment Temperature 2 tool.

Table S3

Main statistics of d-values (A) for the (101) peaks of quartz and opal-CT for repeated (n-6) XRD measurements (in the 15°-30° 2θ range) of selected Site U1545 samples

Sample	quartz (101)	opal-CT (101)
55X_5W_65-75cm	3.342	4.095
	3.343	4.099
	3.344	4.104
	3.343	4.110
	3.342	4.099
	3.342	4.092
Average	3.343	4.100
SD	0.001	0.006
U1545A_63X_4W_	3.341	4.085
	3.332	4.065
	3.332	4.065
	3.332	4.069
	3.333	4.064
	3.340	4.068
Average	3.335	4.069
SD	0.004	0.008
U1545A_65X_3W_	3.336	4.060
	3.340	4.077
	3.334	4.061
	3.334	4.063
	3.339	4.070
	3.340	4.076
Average	3.337	4.068
SD	0.003	0.007
U1545A_65X_5W_	3.323	4.042
	3.329	4.045
	3.328	4.053
	3.329	4.049
	3.328	4.046
	3.329	4.051
Average	3.328	4.048
SD	0.003	0.004
All samples	Quartz (101)	Opal-CT (101)
Average	3.336	4.071
SD	0.003	0.006

Table S3. Main statistics of the d-spacing values (Å) for the (101) peaks of quartz and opal-CT for repeated (n-6) XRD measurements (in the 15º-30º 2θ range) of selected Site U1545 samples.

Table S4 - Comparison between 'classic' and new kinetic models for opal-A/CT transformation and prediction of temperatures for opal-CT precipitation for ~14% slower sedimentation rates															
	Site U1545					Site U1546					Site U1547				
Depth (m)	Age (year)	T of opal-CT (ºC) ('classic' model)	T of opal-CT (ºC) (new kinetic model)	ΔT (ºC) (new kinetic - classic)	T of opal-CT based on 'classic' model with 18% reduced sedimentatio rate (ºC)	Age (year)	T of opal-CT (ºC) ('classic' model)	T of opal-CT (ºC) (new kinetic model)	ΔT (ºC) (new kinetic - classic)	T of opal-CT based on 'classic' model with 18% reduced sedimentatio rate (ºC)	Age (year)	T of opal-CT (ºC) ('classic' model)	T of opal-CT (ºC) (new kinetic model)	ΔT (ºC) (new kinetic - classic)	T of opal-CT based on 'classic' model with 18% reduced sedimentatio rate (ºC)
0	0					0					0				
10	11587	97.78	134.39	36.60	129.64	9804	100.66	137.71	37.05	133.04	19084	89.44	124.77	35.33	0.34
20	23175	86.29	121.15	34.86	116.13	19608	89.00	124.26	35.27	119.30	38168	78.45	112.14	33.69	1.02
30	34762	79.89	113.80	33.91	108.63	29412	82.50	116.80	34.29	111.69	57252	72.33	105.12	32.79	1.74
40	46350	75.49	108.75	33.26	103.49	39216	78.03	111.67	33.63	106.46	76336	68.11	100.29	32.18	2.22
50	57937	72.15	104.92	32.77	99.59	49020	74.65	107.78	33.13	102.50	95420	64.91	96.63	31.72	2.57
60	69525	69.47	101.85	32.38	96.47	58824	71.93	104.66	32.74	99.33	114504	62.34	93.69	31.35	2.85
70	81112	67.23	99.29	32.06	93.87	68627	69.66	102.06	32.41	96.69	133588	60.19	91.24	31.05	3.08
80	92700	65.32	97.10	31.78	91.65	78431	67.72	99.84	32.13	94.43	152672	58.36	89.15	30.79	3.28
90	104287	63.65	95.19	31.54	89.71	88235	66.02	97.91	31.88	92.47	171756	56.76	87.32	30.56	3.45
100	115875	62.17	93.50	31.33	87.99	98039	64.52	96.19	31.67	90.72	190840	55.34	85.70	30.36	3.59
110	127462	60.84	91.99	31.14	86.45	107843	63.18	94.65	31.47	89.16	209924	54.06	84.25	30.18	3.72
120	139050	59.64	90.61	30.97	85.06	117647	61.96	93.26	31.30	87.75	229008	52.91	82.93	30.02	3.84
130	150637	58.54	89.36	30.82	83.79	127451	60.84	91.99	31.14	86.45	248092	51.85	81.73	29.88	3.95
140	162225	57.53	88.20	30.67	82.62	137255	59.82	90.82	31.00	85.27	267176	50.88	80.63	29.74	4.04
150	173812	56.60	87.14	30.54	81.53	147059	58.87	89.73	30.86	84.17	286260	49.99	79.60	29.62	4.13
160	185400	55.73	86.14	30.42	80.53	156863	57.99	88.73	30.74	83.15	305344	49.15	78.65	29.50	4.22
170	196987	54.91	85.22	30.30	79.59	166667	57.16	87.79	30.62	82.19					
180	208575	54.15	84.35	30.20	78.70	176471	56.39	86.90	30.51	81.30					
190	220162	53.43	83.53	30.10	77.87	186275	55.66	86.07	30.41	80.45					
200	231750	52.75	82.75	30.00	77.09	196078	54.97	85.29	30.31	79.66					
210	243337	52.11	82.02	29.91	76.35	205882	54.32	84.54	30.22	78.90					
220	254925	51.50	81.32	29.83	75.64	215686	53.70	83.84	30.13	78.19					
230	266512	50.92	80.66	29.75	74.97	225490	53.11	83.17	30.05	77.51					
240	278100	50.36	80.03	29.67	74.33	235294	52.55	82.53	29.97	76.86					
250	289687	49.83	79.43	29.59	73.72	245098	52.01	81.91	29.90	76.24					
260	301275	49.32	78.85	29.52	73.13	254902	51.50	81.33	29.83	75.64					
270	312862	48.84	78.29	29.46	72.57	264706	51.01	80.76	29.76	75.07					
280	324450	48.37	77.76	29.39	72.03	274510	50.53	80.22	29.69	74.53					
290	336037	47.92	77.25	29.33	71.51	284314	50.07	79.70	29.63	74.00					
300	347625	47.48	76.75	29.27	71.01	294118	49.63	79.20	29.57	73.49					
310	359212	47.07	76.28	29.21	70.53	303922	49.21	78.72	29.51	73.00					
320	370800	46.66	75.82	29.16	70.06	313725	48.80	78.25	29.45	72.53					
330	382387	46.27	75.37	29.10	69.61	323529	48.40	77.80	29.40	72.07					
340	393975	45.89	74.94	29.05	69.18	333333	48.02	77.37	29.34	71.63					
350	405562	45.53	74.53	29.00	68.76	343137	47.65	76.94	29.29	71.20					
360	417149	45.17	74.12	28.95	68.35	352941	47.29	76.53	29.24	70.79					
370	428737	44.83	73.73	28.90	67.95	362745	46.94	76.14	29.19	70.39					
380	440324	44.49	73.35	28.86	67.57	372549	46.60	75.75	29.15	70.00					
390	451912	44.16	72.98	28.81	67.19	382353	46.27	75.37	29.10	69.62					
400	463499	43.85	72.62	28.77	66.83	392157	45.95	75.01	29.06	69.25					
410	475087	43.54	72.27	28.73	66.47	401961	45.64	74.65	29.02	68.89					
420	486674	43.24	71.93	28.69	66.13	411765	45.33	74.31	28.97	68.54					
430	498262	42.95	71.59	28.65	65.79	421569	45.04	73.97	28.93	68.20					
440	509849	42.66	71.27	28.61	65.46	431373	44.75	73.64	28.89	67.86					
450	521437	42.38	70.95	28.57	65.14	441176	44.47	73.32	28.85	67.54					
460	533024	42.11	70.64	28.53	64.83	450980	44.19	73.01	28.82	67.22					
470	544612	41.85	70.34	28.50	64.53	460784	43.92	72.70	28.78	66.91					
480	556199	41.59	70.05	28.46	64.23	470588	43.66	72.40	28.74	66.61					
490	567787	41.33	69.76	28.43	63.94	480392	43.40	72.11	28.71	66.31					
500	579374	41.08	69.48	28.39	63.65	490196	43.15	71.82	28.67	66.02					
510	590962	40.84	69.20	28.36	63.37	500000	42.90	71.54	28.64	65.74					

Table S4. For each of the three IODP Expedition 385 sites examined in this paper we present a comparison between 'classic' (Mizutani et al., 1970) and new kinetic model (the one proposed in this paper) for opal-A/CT transformation. To test the hypothesis that the fast sedimentation rates are responsible for shuttling amorphous silica deeper/older than expected based on current kinetic models we calculated the temperatures for opal-CT precipitation by simulating slower sedimentation rates of about one order of magnitude. The latter was simulated by reducing the time factor (t) in k = -ln(0.9)/t to a value between 0.1 and 0.2. The best fit between observed and modeled data was obtained when we used ~14% slower sedimentation rates.